Materials Research Bulletin 48 (2013) 4261–4266

Contents lists available at SciVerse ScienceDirect

Materials Research Bulletin

journal homepage: www.elsevier.com/locate/matresbu

CdS and CdS/CdSe sensitized ZnO nanorod array solar cells prepared by a solution ions exchange process

Ling Chen [a], Haibo Gong [a], Xiaopeng Zheng [a], Min Zhu [a], Jun Zhang [a],
Shikuan Yang [b], Bingqiang Cao [a,*]

[a] Key Laboratory of Inorganic Functional Materials in Universities of Shandong, School of Materials Science and Engineering, University of Jinan, Jinan 250022, Shandong, China
[b] Department of Engineering Science and Mechanics, The Pennsylvania State University, University Park, PA 16802-6812, USA

ARTICLE INFO

Article history:
Received 24 January 2013
Received in revised form 8 June 2013
Accepted 26 June 2013
Available online 9 July 2013

Keywords:
A. Oxides
B. Chemical synthesis
D. Optical properties

ABSTRACT

In this paper, cadmium sulfide (CdS) and cadmium sulfide/cadmium selenide (CdS/CdSe) quantum dots (QDs) are assembled onto ZnO nanorod arrays by a solution ion exchange process for QD-sensitized solar cell application. The morphology, composition and absorption properties of different photoanodes were characterized with scanning electron microscope, transmission electron microscope, energy-dispersive X-ray spectrum and Raman spectrum in detail. It is shown that conformal and uniform CdS and CdS/CdSe shells can grow on ZnO nanorod cores. Quantum dot sensitized solar cells based on ZnO/CdS and ZnO/CdS/CdSe nanocable arrays were assembled with gold counter electrode and polysulfide electrolyte solution. The CdS/CdSe sensitization of ZnO can effectively extend the absorption spectrum up to 650 nm, which has a remarkable impact on the performance of a photovoltaic device by extending the absorption spectrum. Preliminary results show one fourth improvement in solar cell efficiency.

1. Introduction

The increasing demand of energy imposes us to explore environmentally clean resources for future. Solar energy is one of the most promising resources to solve the predicament of energy shortage. As a typical new kind of solar cell, dye sensitized solar cell (DSSC) has attracted tremendous attention due to their high photovoltaic conversion efficiency up to 12% [1], and offers a possibility of fabricating low-cost, low-energy-consumption solar cell devices [2,3]. Recently, quantum dots like CdS [4], CdSe [5], CdTe [6], and PbS [7] have been investigated as very promising alternative candidates for light absorbers due to the advantages over metalorganic dyes, which include size-dependent band gap [8], high extinction coefficients [8,9] and large intrinsic dipolar moment [10]. On the other hand, one-dimensional (1D) ZnO nanostructures [11–13] like nanorods or nanowires are expected to significantly improve the electron diffusion length by providing a direct conduction pathway for the rapid collection of photo-generated electrons, which have few grain boundaries in comparison with TiO_2 polycrystalline mesoporous film photo-anode. But the efficiency of QD-sensitized solar cell (QDSSC) is still lower than the model of dye sensitized solar cell proposed by O'Regan and Grätzel [2]. How to extend the spectral response range of quantum dots layer and obtain a conformal and uniform quantum dots layer on the surface of ZnO nanorods should be both major challenges to further improve the solar cell efficiency. Many methods have been explored to solve these problems, such as chemical bath deposition (CBD) [14,15], assembling QDs onto the substrate surface using bifunctional molecule linkers [16], successive ionic layer adsorption and reaction (SILAR) [17,18], and electrochemical deposition method [19]. For example, doped colloidal quantum dots with different sizes were assembled to the substrate surface using bifunctional molecules as interconnected linkers [20,21]. However, low QD adsorption on the surface limits the solar cell performance, because partially covered photoanode layer would also cause serious leakage current between the photoanode and electrolyte interface [22].

In this paper, we adopted a facile and low-cost solution process to sensitize ZnO nanorods with pure CdS and CdS/CdSe QD layers. Such CdS/CdSe shell layer was fabricated on the surface of ZnO nanorods by partial substitution of S^{2-} for Se^{2-} in pre-formed CdS layer. This method proves to form conformal and uniform CdS and CdS/CdSe shells on ZnO cores and enables to extend the absorption spectrum range effectively. Accordingly, the CdS/CdSe shell sensitized ZnO nanorods solar cells exhibited better photovoltaic performance than the CdS sensitized cells.

---

* Corresponding author. Tel.: +86 531 89736292; fax: +86 531 87974453.
E-mail address: mse_caobq@ujn.edu.cn (B. Cao).

0025-5408/$ – see front matter © 2013 Elsevier Ltd. All rights reserved.
http://dx.doi.org/10.1016/j.materresbull.2013.06.069

2. Experimental

2.1. Growth of ZnO nanorods

ZnO nanorods array were prepared by hydrothermal growth route on FTO glasses with sheet resistance of 14 Ω sq^{-1}. Prior to the synthesis of ZnO nanorods array, the FTO glasses were cleaned with isopropanol, ethanol by ultrasonication sequentially. Then ZnO seed layers were deposited by spin coating with ethylene glycol monomethylether solution containing 40 mM zinc acetate dehydrate ($Zn(CH_3COOH)_2{\cdot}2H_2O$) and 40 mM ethanolamine at a speed of 3500 rpm for 40 s. This step was repeated two times and then the substrates were heated at 500 °C in air for 60 min to form a ZnO seed layer. The ZnO nanorods were grown by immersing the seeded substrates in aqueous solutions containing 25 mM zinc nitrate hydrate ($Zn(NO_3)_2{\cdot}6H_2O$) and 25 mM hexamethylenetetramine (HMAT) at 90 °C for 10 h. The ZnO nanorods were annealed at 500 °C for 60 min in air after growth.

2.2. Growth of ZnO/CdS and ZnO/CdS/CdSe core/shell nanocable

First, ZnO nanorods were immersed in the aqueous solution containing 0.1 M $Na_2S{\cdot}9H_2O$ for 10 min at room temperature to form a thin ZnS layer on the surface of ZnO nanorods by exchanging O^{2-} with S^{2-}. Then the samples were rinsed with deionized water and ethanol. Second, the samples were further immersed in the aqueous solution containing 25 mM cadmium nitrate ($Cd(NO_3)_2$), 0.1 M thiourea, and 0.1 M ethylenediamine for 60 min at room temperature to form ZnO/CdS nanocable array. Finally, to prepare ZnO/CdS/CdSe nanocable arrays, the ZnO/CdS nanocable array were immersed in a 30 mL aqueous solution containing 0.015 g of Se and 0.05 g of $NaBH_4$ at 90 °C for 120 min by partial substitution Se^{2-} for S^{2-}, and then the samples were rinsed with deionized water and ethanol for further characterization or device fabrication.

2.3. Fabrication of CdS and CdS/CdSe sensitized ZnO nanorods solar cells

The fresh polysulfide electrolyte was prepared by dissolving 0.50 M Na_2S, 2.0 M sulfur, and 0.20 M KCl into water/methanol (3:7, v/v) solution [23]. Gold counter electrode was prepared by DC sputtering method on clean FTO glass slides with a deposition current of 30 mA for 200 s. The solar cells were assembled by attaching the anode electrode and counter electrode with a thermoplastics biphenylframe (Surlyn, 25 μm thick). The electrolyte was introduced through a predrilled hole and then the hole was sealed with a cover slide. The active area of the solar cell was 0.6 cm × 0.6 cm.

2.4. Sample characterization and device evaluation

The morphologies of the samples were examined with a Quanta FEG250 field emission scanning electron microscope (FE-SEM) and the nanocable microstructures were analyzed with transmission electron microscope (TEM, Philips CM 20) and high-resolution TEM (HRTEM, JEOL JEM-2100F) both operated at 200 kV. The element composition analysis was performed with energy-dispersive X-ray spectrum (EDX, Inca, Oxford). The UV–vis absorption spectrum was recorded by a Shimadzu UV-3101PC spectrophotometer. Raman spectral analysis was performed at room temperature with a confocal microprobe Raman system (LABRAM-HR). The excitation source was 514.5 nm light of argon ion laser. For photoluminescence (PL) measurements, 313 nm light from a Xenon lamp as excitation source was focused on the sample through an optical chopper (SR 540). The PL signal dispersed by a monochrometer was detected by a photomultiplier (PMTH-S1-CR131) through a lock-in amplifier (SR 830). Photovoltaic measurements were recorded employing a 3A solar simulator (XES-40S1, San-Ei) with an AM 1.5 spectrum distribution. The power of the light was calibrated against a standard ISE CalLab Fraunhofer silicon solar cell to accurately simulate one full-sun intensity (100 mW/cm^2). The solar cells were fixed on a temperature-controlled sample test stage (0821, Vision-Tec) to keep the devices at a temperature of 25 °C. The current–voltage (J–V) characteristics of the samples were measured with a Keithley 2612A source/meter. External quantum efficiency (EQE) of the devices was measured with QEX10 solar cell spectral response equipment (PV Measurement).

3. Results and discussion

3.1. Morphology and composition characterization

Fig. 1(a) and (b) shows the morphology of ZnO nanorods grown on seeded FTO-glass substrates. The diameters of nanorods are in a range of 50–100 nm with a height of 2 μm. Such nanorods have smooth surfaces with hexagonal flat tips as shown in the inset of Fig. 1(a). The inset of Fig. 1(b) shows a typical PL spectrum of ZnO nanorods at room temperature. The near band UV emission peak at about 383 nm is higher than the green emission peak, which is generally observed for ZnO due to some intrinsic defects like oxygen vacancy or zinc interstitial [24,25]. This indicates the high crystal quality of ZnO nanorods obtained by hydrothermal growth method. This would benefit photocarriers transmission along such

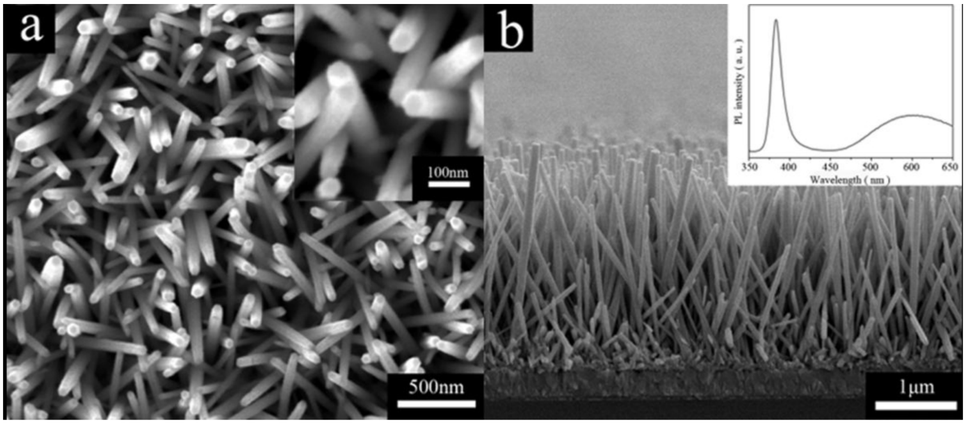

Fig. 1. (a) Top-view SEM image of ZnO nanorods with enlarged image as inset; (b) cross-sectional SEM image of ZnO nanorods with an typical PL spectrum of the ZnO nanorods as inset.

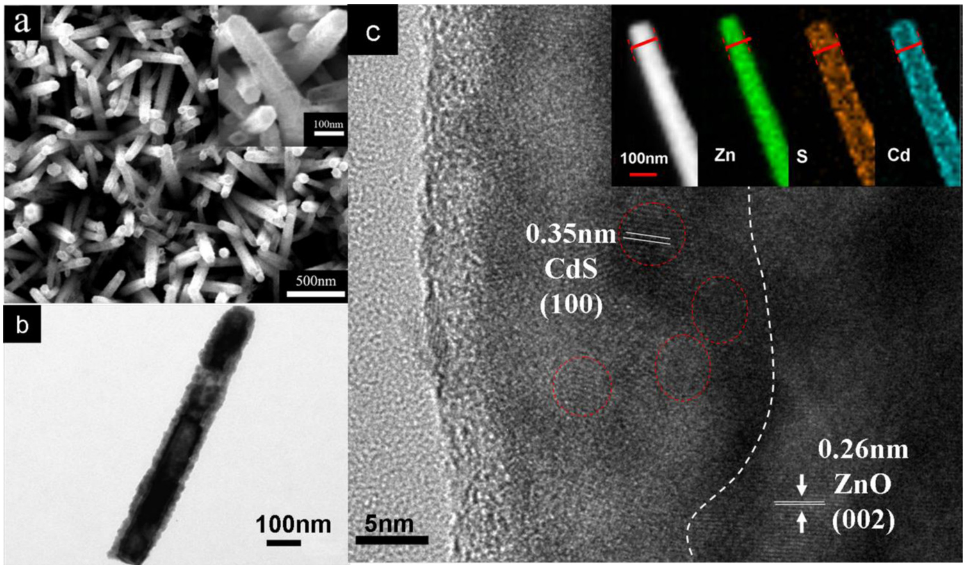

Fig. 2. (a) Top-view and enlarged view SEM images of ZnO/CdS nanocable array; (b) TEM image of a ZnO/CdS nanocable; (c) HRTEM image obtained at the surface region of a ZnO/CdS core/shell nanocable and EDX mappings of Zn, S, and Cd elements shown in inset of (c). Dashed circles are indicated for CdS QDs.

nanorods and decrease series resistance for the later assembled solar cells.

A SEM image of ZnO/CdS nanocable array is shown in Fig. 2(a). We can find that the nanorod surfaces become rougher after CdS shell growth in comparison with Fig. 1(a). TEM observation in Fig. 2(b) reveals that a conformal and uniform shell layer of about 20 nm is grown on the surface of ZnO nanorod. Close observation by HRTEM demonstrates that the shell is composed of nanoparticles of about 4–5 nm in diameter, as depicted in Fig. 2(c). The calculated lattice spacing of the nanoparticles is about 0.35 nm, which is consistent with that of hexagonal CdS. To further study the chemical composition of shell layer, EDX elemental mappings were detected as shown in the inset of Fig. 2(c), which exhibits the uniform Cd and S mappings along the whole ZnO nanorod. The distribution of Cd and S are about 20 nm thicker than of that of Zn mapping, which indicates that the CdS shell growth on the surface ZnO nanorod.

After further immersion of the ZnO/CdS nanorods into Se^{2-} source solution, the surface of the nanocable became rougher as shown in Fig. 3(a). TEM observation in Fig. 3(b) reveals that a conformal and uniform shell layer ~20 nm is still preserved on the surface of ZnO nanorod. HRTEM image as shown in Fig. 3(c) shows that shell layer is composed of ~4 nm CdS and ~5 nm CdSe QDs. Both the orientation and distribution of CdS and CdSe QDS are random as indicated by the lattice spacings and fringes. Due to the exchange of S^{2-} ions with Se^{2-} ions, a CdSe QD layer of about 7 nm is grown as the outmost layer and the CdS layer is reduced to 13 nm. The shell layer was further characterized by EDX mapping as shown in inset of Fig. 3(c). The distribution thickness of Zn element is smaller than those of S, Se and Cd. Meanwhile, the signal

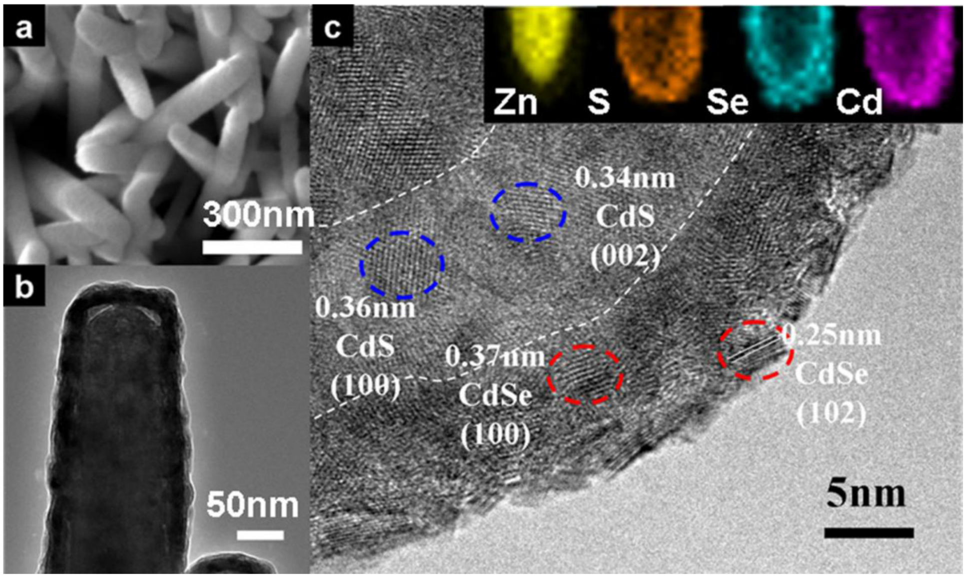

Fig. 3. (a) Top-view SEM image of ZnO/CdS/CdSe nanocable array; (b) TEM image of a ZnO/CdS/CdSe nanocable; (c) HRTEM image obtained at the surface region of a ZnO/CdS/CdSe core/shell nanocable and EDX mappings of Zn, S, Se, and Cd shown in inset of (c). Dashed lines and circles are indicated for shell layer interface and different QDs.

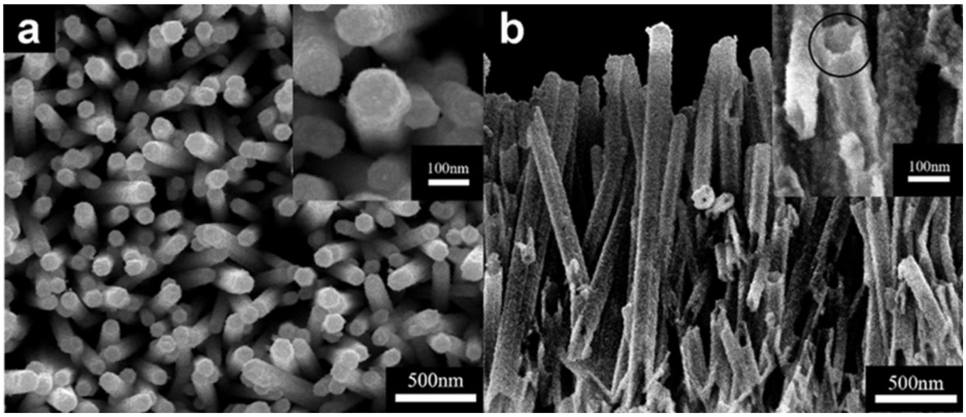

Fig. 4. (a) Top-view SEM of CdS/CdSe nanotubes fabricated by corrosion of ZnO/CdS/CdSe nanocable array in acetic acid for 2 h; (b) Cross-sectional SEM image of CdS/CdSe nanotubes; insets are the corresponding partial enlarged view.

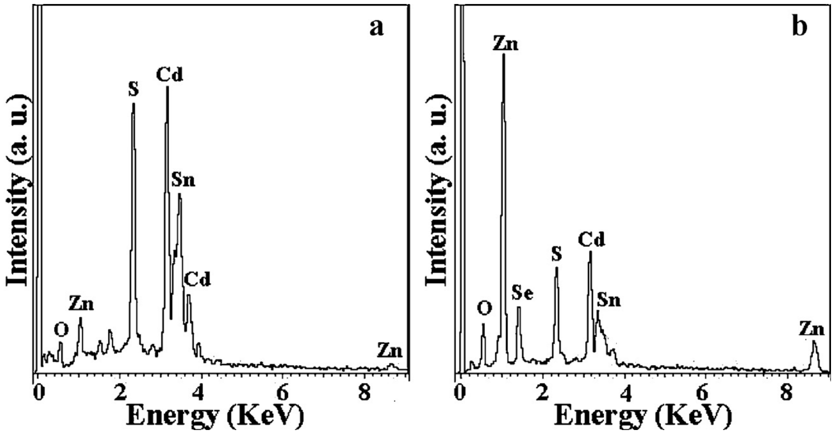

Fig. 5. The EDX spectra of (a) CdS nanotubes and (b) CdS/CdSe nanotubes as shown in Fig. 4.

intensities of S and Se are deeper in the edge than the center. These further indicate that the core and shell of nanocable are composed of ZnO and CdS/CdSe QDs layer, respectively.

To further check the component of the QD shell, the ZnO core was etched away. Fig. 4(a) and (b) shows the morphology of CdS/CdSe nanotubes after etching the ZnO cores away in an acetic acid solution, where the tops of CdS/CdSe nanotubes are sealed and the tubular structure is only found from the fracture of nanotubes. It indicates that the corrosion of CdS/CdSe nanocable array first happen from the roots without shells coating. It further proves the conformal CdS/CdSe shell growth onto the nanorod that can protect ZnO core from acid corrosion. This can also prevent the direct contact between ZnO nanorods and electrolyte, which effectively suppress the current leakage at the photoanode and electrolyte interface.

For analysis accuracy, the EDX measurements of CdS and CdS/CdSe shells were performed with a large-area scanning mode as shown in Fig. 5. Besides the Sn, O and Zn signals from the substrate and left ZnO cores, only Cd and S elements with an approximate atomic ratio of 1:1 are detected as shown in Fig. 5(a), which indicates that a uniform CdS shell layer grows on the ZnO nanorods surface for ZnO/CdS samples. For ZnO/CdS/CdSe nanocable sample, the atom sum of sulfur and selenium is much more than that of cadmium that is constant during the chemical etching process. The reason is that the thicker CdS/CdSe shell as shown in Fig. 3(b) can

Table 1
EDX analysis of CdS and $CdS_{0.58}/CdSe_{0.42}$ nanoshells.

Element (at%)	Zn	Sn	Cd	O	S	Se	Total
CdS nanotubes	4.99	15.80	25.69	28.09	25.43	–	100
CdS_xSe_{1-x} nanotubes	31.46	3.29	13.54	34.21	11.86	5.64	100

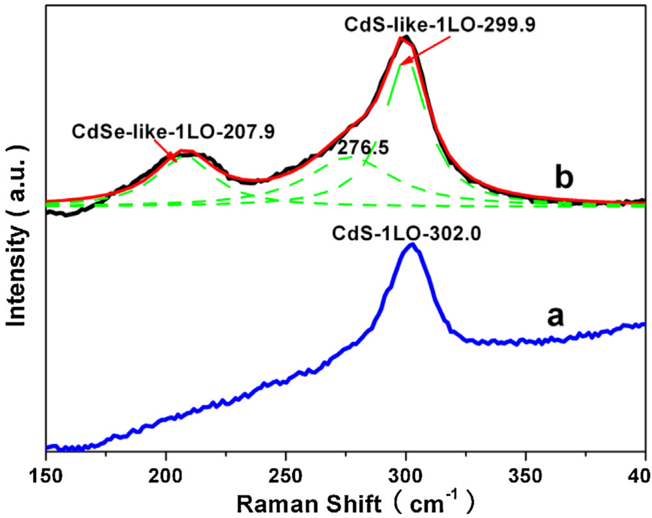

Fig. 6. (a) The Raman spectrum of ZnO/CdS nanocable (the blue solid line). (b) The Raman spectrum of $ZnO/CdS_{0.58}/CdSe_{0.42}$ nanocable (the dark solid line), the red and green lines are the Lorentz fitting results. (For interpretation of the references to color in this figure legend, the reader is referred to the web version of the article.)

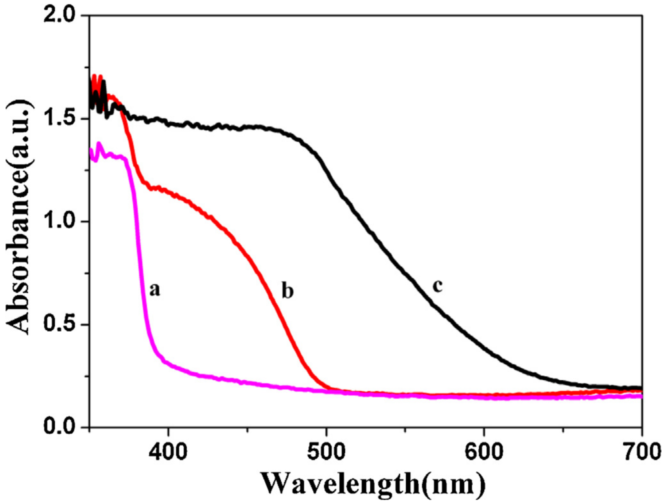

Fig. 7. The UV–vis absorption spectra of (a) ZnO nanorods, (b) ZnO/CdS nanocable, (c) ZnO/$CdS_{0.58}$/$CdSe_{0.42}$ nanocable.

prevent the nanorod core from etching more effectively within the same corrosion time, which further proves the conformal coating on nanorods is realized by such a solution method. Using the cadmium as a benchmark, the calculated ratio of S and Se is 58:42 in CdS/CdSe ($CdS_{0.58}$/$CdSe_{0.42}$) shell (Table 1).

The formation and composition of CdS and $CdS_{0.58}$/$CdSe_{0.42}$ shells on the ZnO nanorods were further confirmed by Raman spectroscopy, as shown in Fig. 6. For the ZnO/CdS nanocable (spectrum a), the Raman peak at 302.0 cm^{-1} corresponds to the first order longitudinal optical (LO) phonon mode of CdS [26]. It proves the formation of pure CdS shell. After the exchange reaction with Se^{2-}, a new prominent mode (spectrum b) at 207.9 cm^{-1} that is attributed to the first order LO mode of CdSe appears together with the CdS-LO mode at 299.9 cm^{-1}. The low-energy shoulder may originate from the surface optical phonon mode as observed in CdS@CdSe core–shell QDs [27]. Moreover, the CdS-LO peak asymmetry and down-shift of ZnO/$CdS_{0.58}$/$CdSe_{0.42}$ are both more clear than those of ZnO/CdS due to the phonon confinement effect [28]. This could be due to the reduction of CdS crystallite size caused by the partial formation of CdSe QDs [29].

3.2. Optical properties of ZnO/CdS and ZnO/$CdS_{0.58}$/$CdSe_{0.42}$ nanocable

Fig. 7 shows the UV–vis absorption spectra of ZnO nanorods, ZnO/CdS and ZnO/$CdS_{0.58}$/$CdSe_{0.42}$ nanocable arrays. Fig. 7(a) exhibits a clear absorption edge of ZnO nanorods at about 380 nm, which corresponds to the electron transition from top of valence band to bottom of conduction band. After the formation of CdS shells on the nanorods, the absorption edge of ZnO/CdS nanocables extends to 500 nm due to the effective absorption of CdS shell with a bandgap of 2.5 eV. After the formation of $CdS_{0.58}$/$CdSe_{0.42}$ shells by partial conversion of CdS to CdSe QDs, the absorption edge further shifted to 650 nm. Consequently, the extending of absorption edge from UV to visible region is realized by formation ZnO/$CdS_{0.58}$/$CdSe_{0.42}$ nanocable. It is also important to note that the ZnO/$CdS_{0.58}$/$CdSe_{0.42}$ nanocable array shows a gradual absorption onset, indicating ploydispersed sizes of $CdS_{0.58}$/$CdSe_{0.42}$ nanocrystals in the nanorod shell [30].

Table 2
Photovoltaic performance of CdS and $CdS_{0.58}$/$CdSe_{0.42}$ sensitized ZnO solar cells.

Sample	J_{sc} (mA/cm^2)	V_{oc} (V)	FF (%)	η (%)
ZnO/CdS	2.51	0.34	34.67	0.29
ZnO/$CdS_{0.58}$/$CdSe_{0.42}$	3.20	0.39	28.76	0.36

3.3. Photovoltaic characteristics of ZnO/CdS and ZnO/$CdS_{0.58}$/$CdSe_{0.42}$ QDSSCs

Fig. 8 shows current density–voltage (*J–V*) curves and external quantum efficiency (EQE) spectra of ZnO/CdS and ZnO/$CdS_{0.58}$/$CdSe_{0.42}$ solar cells. For comparison, detailed photovoltaic parameters, e.g. the short-circuit density (J_{sc}), open-circuit voltage (V_{oc}), fill factor (FF), and photovoltaic conversion efficiency (η), are summarized in Table 2. The solar cells were assembled using gold counter electrode and polysulfide redox couple and measured under standard one-sun irradiation with AM 1.5 spectrum distribution without masking. The *J–V* curves in Fig. 8(a) show that both the J_{sc} and V_{oc} of $CdS_{0.58}$/$CdSe_{0.42}$ sensitized solar cell increase slightly in comparison with those of CdS sensitized solar cell. Therefore, the power conversion efficiency (η) increases from 0.29% to 0.36%. The increase of J_{sc} may be ascribed to the improved light absorption after the partial conversion of CdS to CdSe. This is further approved by the EQE spectra of the corresponding cells, as shown in Fig. 8(b). The formation of $CdS_{0.58}$/$CdSe_{0.42}$ shells on ZnO cores enables to extend the spectrum region up to 650 nm, which is consistent with the UV–vis absorption spectra. But the EQE of $CdS_{0.58}$/$CdSe_{0.42}$ sensitized solar cell is lower than that of CdS sensitized solar cell when the incident photon wavelength is shorter than 500 nm. The possible reason is that the defects in $CdS_{0.58}Se_{0.42}$ shell caused by the substitution of S^{2-} with Se^{2-} acting as recombination center leading to the recombination of photoexcited electrons and holes directly before separation. Accordingly, the fill factor is also reduced from 34.67% to 28.76%

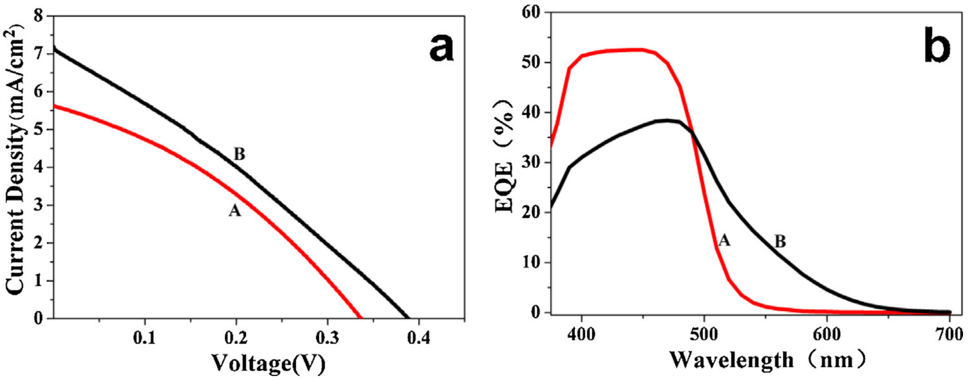

Fig. 8. (a) The *J–V* curves and (b) EQE spectra of two QD sensitized solar cells, curve A for CdS sensitized ZnO solar cell and curve B for $CdS_{0.58}Cd/Se_{0.42}$ sensitized ZnO solar cell.

as shown in Table 2. Moreover, ZnO nanorods partially peeling from the FTO-glass substrate due to the corrosion in an alkaline solution (pH $\approx$ 13) was also observed (not shown here) when CdS shells grew onto ZnO nanorods. This could cause current leakage at the interfaces between FTO-glass substrate and electrolyte also leading to a poor photovoltaic performance. Therefore, a compact blacking layer introduced between the glass substrate and ZnO nanorods should reduce the current leakage and therefore increase the solar cell efficiency. Moreover, the thickness optimization of CdS/CdSe QD layer should also be important for further efficiency enhancement.

4. Conclusion

In summary, we have shown that through a simple room-temperature chemical solution ion exchange method, a uniform and conformal coating of ZnO nanorods with CdS and $CdS_{0.58}/CdSe_{0.42}$ shells can be achieved. Dipping the ZnO nanorods into sulfide precursor results in partial conversion of ZnO to ZnS nanorods. The ZnS promotes nucleation of CdS shells compared to ZnO nanorods and $CdS_{0.58}/CdSe_{0.42}$ shells can further grow on ZnO nanorod cores by partial substitution of S^{2-} with Se^{2-}. Such CdS and CdS/CdSe sensitized photoanodes were adopted for QD-sensitized solar cell application. A remarkable impact on the performance of a photovoltaic device was observed by extending the absorption spectrum. Preliminary results show one fourth improvement in solar cell efficiency. However, the power conversion efficiency was still low. Further effort is in great need to solve several problems like current leakage between FTO glass and electrolyte and defects in the $CdS_{0.58}/CdSe_{0.42}$ shell. Such work is undergoing in our lab.

Acknowledgements

This work is supported by NSFC (51002065, 11174112) and Shandong Provincial Science Foundation for Disguised Youth Scholars (2012JQB01031; BS2010CL003). The Program for New Century Excellent Talents in University (NCET-11-1027), Ministry of Education, China, is also acknowledged. BC thanks the Taishan Scholar Professorship (TSHW20091007) tenured at University of Jinan.

References

[1] M.K. Nazeeruddin, F.D. Angelis, S. Fantacci, A. Selloni, G. Viscardi, P. Liska, S. Ito, B. Takeru, M. Grätzel, J. Am. Chem. Soc. 127 (2005) 16835–16847.

[2] B. O'Regan, M. Grätzel, Nature 353 (1991) 737–740.

[3] M. Grätzel, Nature 414 (2001) 338–344.

[4] W.T. Sun, Y. Yu, H.Y. Pan, X.F. Gao, Q. Chen, L.M. Peng, J. Am. Chem. Soc. 130 (2008) 1124–1125.

[5] A. Kongkanand, K. Tvrdy, K. Takechi, M. Kuno, P.V. Kamat, J. Am. Chem. Soc. 130 (2008) 4007–4015.

[6] J.A. Seabold, K. Shankar, R.H.T. Wilke, M. Paulose, O.K. Varghese, C.A. Grimes, K.S. Choi, Chem. Mater. 20 (2008) 5266–5273.

[7] B.R. Hyun, Y.W. Zhong, A.C. Bartnik, L. Sun, H.D. Abruna, F.W. Wise, J.D. Goodreau, J.R. Matthews, T.M. Leslie, N.F. Borrelli, ACS Nano 2 (2008) 2206–2212.

[8] W.W. Yu, L.H. Qu, W.Z. Guo, X.G. Peng, Chem. Mater. 5 (2003) 2854–2860.

[9] P. Wang, S.M. Zakeeruddin, M. Grätzel, Adv. Mater. 16 (2004) 1806–1811.

[10] R.D. Schaller, M. Sykora, J.M. Pietryga, V.I. Klimov, Nano Lett. 6 (2006) 424–429.

[11] W.W. Wu, G.D. Hu, S.G. Cui, Y. Zhou, H.T. Wu, Cryst. Growth Des. 8 (2008) 4014–4020.

[12] P. Zhang, G.D. Zhou, H.B. Gong, H.Y. Xu, D. Nakamura, T. Okada, H.B. Zeng, B.Q. Cao, Sci. Adv. Mater. 4 (2012) 455–462.

[13] H.B. Zeng, J.B. Cui, B.Q. Cao, U. Gibson, Y. Bando, D. Golberg, Sci. Adv. Mater. 2 (2010) 336–358.

[14] C.H. Chang, Y.L. Lee, Appl. Phys. Lett. 91 (2007) 053503–053505.

[15] E. Edri, E. Rabinovich, O. Niitsoo, H. Cohen, T. Bendikov, G. Hodes, J. Phys. Chem. C 114 (2010) 13092–13097.

[16] K.S. Leschkies, R. Divakar, D.J. Norris, E.S. Aydil, Nano Lett. 7 (2007) 1793–1798.

[17] H. Lee, M.K. Wang, P. Chen, D.R. Gamelin, S.M. Zakeeruddin, M. Grätzel, M.K. Nazeeruddin, Nano Lett. 9 (2009) 4221–4227.

[18] Y.L. Lee, Y.S. Lo, Adv. Funct. Mater. 19 (2009) 604–609.

[19] R.T. Zaera, A. Katty, S. Bastide, C.L. Clément, Chem. Mater. 19 (2007) 1626–1632.

[20] Z.S. Yang, H.T. Chang, Sol. Energy Mater. Sol. Cells 94 (2010) 2046–2051.

[21] A. Ruland, C.S. Drost, V. Sgobba, D.M. Guldi, Adv. Mater. 23 (2011) 4573–4577.

[22] G.Y. Lan, Z. Yang, H.T. Chang, J. Mater. Chem. 19 (2009) 2349–2355.

[23] Y.L. Lee, C.H. Chang, J. Power Sources 185 (2008) 584–588.

[24] B.Q. Cao, W.P. Cai, H.B. Zeng, G.T. Duan, Appl. Phys. Lett. 99 (2006) 073516–073522.

[25] B.Q. Cao, W.P. Cai, H.B. Zeng, Appl. Phys. Lett. 16 (2006) 161101–161103.

[26] N. Tschirner, H. Lange, A. Schliwa, A. Biermann, C. Thomsen, K. Lambert, R. Gomes, Z. Hens, Chem. Mater. 24 (2012) 311–318.

[27] A. Roy, A.K. Sood, Phys. Rev. B 53 (1996) 12127–12132.

[28] A.V. Gomonnai1, Y.M. Azhniuk, V.O. Yukhymchuk, M. Kranjčec, V.V. Lopushansky, Phys. Stat. Sol. (b) 239 (2003) 490–499.

[29] D. Bersan, P.P. Lottici, Phys. Stat. Sol. (b) 174 (1992) 575–582.

[30] Z.Z. Lu, J. Xu, X. Xie, H.K. Wang, C.D. Wang, S.Y. Kwok, T.L. Wong, H.L. Kwong, I. Bello, C.S. Lee, S.T. Lee, W.J. Zhang, J. Phys. Chem. C 116 (2012) 2656–2661.